

Trans-Arctic route feasibility on a pan-Arctic grid under bathymetric and sea-ice constraints

Abdella Mohamed^{a,b,*}, Xiangyu Hu^{a,*}

^a*Technical University of Munich, Boltzmannstraße 15, 85748, Garching, Germany*

^b*Everllence (formerly: MAN Energy Solutions), Stadtbachstraße 1, 86153, Augsburg, Germany*

Abstract

Climate-driven reductions in Arctic sea-ice extent have renewed interest in trans-Arctic shipping, yet adoption remains limited by questions of route feasibility, safety, and excess distance. Existing work often compares idealised great-circle shortcuts or uses detailed weather-routing systems that couple metocean forcing, sea ice and ship performance, leaving a gap for basin-scale diagnostics on realistic bathymetry and sea-ice fields. We develop an offline graph-based framework for trans-Arctic route feasibility on a 0.5° pan-Arctic grid that combines General Bathymetric Chart of the Oceans (GEBCO) 2024 bathymetry with a summer 2018 Arctic sea-ice reanalysis from the Copernicus Marine Environment Monitoring Service (CMEMS). Bathymetry is re-gridded to construct sea-only and depth-feasibility masks, while daily sea-ice concentration (SIC) fields define ice-feasibility masks. An A* pathfinding algorithm is applied to a canonical Europe–Asia origin–destination pair to

*Corresponding author

Email addresses: mohamed.abdella@tum.de (Abdella Mohamed),
xiangyu.hu@tum.de (Xiangyu Hu)

quantify route availability and route-length inflation relative to great-circle baselines.

Enforcing sea-only feasibility increases route length by about 10% before depth and ice constraints are applied. At 0.5° resolution, depth thresholds representative of under-keel clearance ($h_{\min} = 20\text{--}50$ m) remove up to roughly 15% of the sea mask but preserve a trans-Arctic connection for $h_{\min} = 20$ m. Summer sea ice exerts a strong seasonal control: continuous ice-safe routes emerge only from mid-August, with distances inflated by roughly 20–25% even in late summer only about 75% of sea cells are simultaneously depth- and ice-safe, leaving no continuous joint-safe trans-Arctic route in the tested season. These diagnostics position the framework as a basin-scale screening tool for Arctic shipping and as a baseline for subsequent forecast-driven, multi-objective Arctic routing studies.

Keywords: Arctic shipping, trans-Arctic routes, sea-ice concentration, bathymetry, graph-based routing, A* pathfinding

Nomenclature

A*	A-star shortest path algorithm
CMEMS	Copernicus Marine Environment Monitoring Service
CMIP	Coupled Model Intercomparison Project
CO ₂	Carbon dioxide
GC	Great-circle
GEBCO	General Bathymetric Chart of the Oceans
NEP	Northeast Passage
NETCDF	Network Common Data Form

NSR	Northern Sea Route
OD	Origin–destination
SIC	Sea-ice concentration
SUEZ	Suez Canal Route
WMO	World Meteorological Organization

1. Introduction

Growing interest in decarbonisation, shifting trade patterns and declining Arctic sea-ice extent have renewed attention to high-latitude shipping corridors linking northern Europe and northeast Asia (Stroeve et al., 2012; Notz and Stroeve, 2016). Trans-Arctic options such as the Northern Sea Route (NSR) and related passages are often presented as 30–40% “shortcuts” relative to traditional Suez route, with implied savings in time, fuel and CO₂ emissions (Melia et al., 2016). At the same time, regulatory uncertainty, sparse infrastructure and safety concerns have so far limited large-scale commercial uptake (Stephenson et al., 2013; Chen et al., 2021).

A growing body of research has examined different aspects of Arctic route feasibility and potential, but important gaps remain at basin scale under explicit bathymetry and sea-ice constraints. One strand uses climate model projections and simple sea-ice indices to map potential future Arctic navigability, typically in terms of seasonal windows or navigable fractions of predefined corridors (Stephenson et al., 2013; Melia et al., 2016; Aksenov et al., 2017; Chen et al., 2021; Zhang et al., 2023). These studies highlight the strong sensitivity of Arctic shipping potential to greenhouse-gas scenarios and ice thresholds, but usually do not construct explicit ship routes on realistic coastal and bathymetric grids. A second strand focuses on detailed techno-economic assessments along specific Arctic routes, combining assumed voyage distances with fuel, emissions and cost models to compare NSR and Suez itineraries under various ice and regulatory regimes (Zhu et al., 2018; Pruyn and van Hassel, 2022). A third strand embeds sea-ice and metocean information directly in operational weather-routing or ship-ice interaction tools, coupling environmental forcing with vessel performance and optimisation algorithms to produce case-specific routes or risk metrics (Kuuliala et al., 2017; Lu et al., 2021; Liu et al., 2023). While powerful, such systems

are often complex and vessel-specific, making them less suited to transparent, basin-scale diagnostics.

Beyond these strands, many corridor-scale comparisons between Arctic and traditional Europe–Asia routes still rely on great-circle or waypoint-based sea-only distances to infer changes in voyage time, fuel consumption and CO₂ emissions between NSR, Suez and Cape of Good Hope baselines. In most such studies, route feasibility is handled implicitly through the placement of waypoints, without explicit bathymetric or sea-ice safety masks. From the perspective of end-users such as shipowners, cargo interests and policy analysts, there remains a need for simpler, physically grounded diagnostics that answer two prior questions: (i) does a continuous trans-Arctic connection exist at all under basic depth and ice criteria, and (ii) if so, what is the associated distance penalty relative to a great-circle lower bound?

This paper aims to bridge part of that gap by developing an offline, graph-based routing framework for historical trans-Arctic route diagnostics under explicit bathymetric and sea-ice constraints. We consider a pan-Arctic corridor from 40°N to 85°N and 20°W to 180°E discretised at 0.5° resolution, and combine GEBCO 2024 bathymetry with a daily Arctic sea-ice concentration (SIC) reanalysis from the Copernicus Marine Environment Monitoring Service (CMEMS) for the June–September 2018 season. A canonical Europe–Asia origin–destination pair is chosen to span the basin without tying the analysis to particular ports, in line with recent work emphasising generic corridor diagnostics over case-specific itineraries (Zhang et al., 2023). On this grid we construct sea-only, depth-constrained, ice-constrained and joint depth-plus-ice feasibility masks, and apply an A* pathfinding algorithm to quantify route availability, distance and excess length relative to great-circle baselines.

The analysis is intentionally restricted to static bathymetry and summer 2018 SIC fields, without metocean forcing, forecasts or vessel-specific performance models. This keeps the framework simple enough for exhaustive seasonal and threshold-sensitivity experiments, and positions the results as an envelope of what is theoretically possible under idealised operational behaviour. At the same time, the use of realistic coastlines, modern bathymetry and regridded sea-ice fields ensures that the diagnostics reflect key physical constraints on large-scale Arctic shipping rather than purely geometric great-circle arguments. The formulation is intended to complement, rather than compete with, more detailed operational weather-routing and techno-economic tools.

More concretely, we address the following questions:

1. How much does enforcing strict sea-only feasibility on a realistic bathymetric grid increase trans-Arctic route length relative to a great-circle baseline?
2. To what extent do simple depth thresholds, representing under-keel clearance for deep-draught vessels, further fragment or constrain basin-scale connectivity at 0.5° resolution?
3. How do summer 2018 sea-ice conditions control the seasonal opening and closing of an ice-safe trans-Arctic corridor, and what distance penalty do they impose relative to the sea-only benchmark?
4. How sensitive are these diagnostics to the assumed sea-ice concentration threshold used to define ice-safe waters?
5. What is the combined impact of bathymetry and sea ice when both depth and ice-safety constraints are enforced simultaneously?

The contributions of the paper are twofold. Methodologically, it proposes a transparent, reproducible workflow for constructing and interrogating safety-constrained routing masks on a pan-Arctic grid, using widely available bathymetric and sea-ice products and a standard graph-search algorithm. From an application perspective, it quantifies how static bathymetry and summer 2018 ice fields jointly shape the feasibility, timing and excess distance of trans-Arctic routes in a summer season, and delineates parameter ranges (season, ice threshold, depth constraint) for which basin-scale connectivity is promoted or suppressed. The framework is designed to serve as a baseline for subsequent work that will add time-dependent forcing, vessel performance models and multi-objective cost functions.

2. Data and methods

2.1. Study domain and routing grid

The analysis focuses on a pan-Arctic corridor that is sufficiently wide to encompass candidate trans-Arctic connections between northern Europe and the North Pacific, while remaining compact enough for systematic grid-based diagnostics. We define a latitude band from 40° N to 85° N and a longitude range from 20° W to 180° E (hereafter referred to as the *routing domain*). This choice captures the Norwegian and Barents Seas, the Arctic Ocean, and the Bering and Okhotsk Seas, together with the adjacent shelves and

marginal seas that are relevant for Europe–Asia traffic, but excludes lower-latitude subtropical waters that are not part of realistic Arctic diversions.

Within this domain we construct a regular latitude–longitude routing grid with a resolution of $\Delta\varphi = \Delta\lambda = 0.5^\circ$, corresponding to a nominal horizontal spacing of approximately 55 km at Arctic mid-latitudes. Grid-cell centres are defined on

$$\begin{aligned}\varphi_i &= 40.5^\circ \text{ N}, 41.0^\circ \text{ N}, \dots, 84.5^\circ \text{ N}, \\ \lambda_j &= 19.5^\circ \text{ W}, 19.0^\circ \text{ W}, \dots, 179.5^\circ \text{ E},\end{aligned}$$

yielding 89×399 grid points. This resolution is a compromise: it is coarse enough to allow efficient A* routing and seasonal sensitivity experiments over the full pan-Arctic corridor, yet fine enough to resolve the major shelf breaks, islands and basin-scale geometrical constraints that modulate trans-Arctic connectivity.

All routing computations operate on this coarse grid. High-resolution datasets (bathymetry and sea-ice concentration) are first subsetting to the routing domain and then mapped onto the 0.5° grid via bilinear interpolation in latitude–longitude space (Sections 2.2 and 2.3). The resulting fields provide, for each routing cell, (i) a static ocean depth, (ii) a static land/sea mask derived from bathymetry, and (iii) a time-dependent sea-ice concentration. These fields are then combined into binary feasibility masks that encode which grid cells may be used by the pathfinding algorithm under different safety assumptions (Sections 2.4–2.5).

2.2. Bathymetry dataset and land/sea mask

Static seafloor topography is taken from the GEBCO 2024 global grid (GEBCO Bathymetric Compilation Group, 2024), subsetting to the routing domain ($40\text{--}85^\circ \text{ N}$, $20^\circ \text{ W--}180^\circ \text{ E}$). The native product has a nominal resolution of 15 arcsec; within the subset, depth values (variable `elevation`) span from approximately -8700 m (deep ocean) to $+5500$ m (continental terrain and ice sheets).

For routing purposes we regrid GEBCO onto the 0.5° routing grid. For each routing cell centre (φ_i, λ_j) , depth is obtained by bilinear interpolation in latitude and longitude, yielding a depth field h_{ij} with shape 89×399 . We adopt the GEBCO sign convention (negative values over the ocean, positive

over land and ice). A binary land/sea mask is then defined as

$$M_{ij}^{\text{sea}} = \begin{cases} 1, & h_{ij} < 0 \text{ m}, \\ 0, & h_{ij} \geq 0 \text{ m}, \end{cases} \quad (1)$$

so that $M^{\text{sea}} = 1$ denotes ocean and $M^{\text{sea}} = 0$ denotes land or grounded ice. This mask defines the maximum set of cells that can ever be used by a route; all subsequent depth and sea-ice constraints operate within $M^{\text{sea}} = 1$.

To represent under-keel clearance requirements we further define depth-thresholded sea masks. Given a minimum acceptable water depth h_{min} , we consider

$$M_{ij}^{\text{depth}}(h_{\text{min}}) = \begin{cases} 1, & M_{ij}^{\text{sea}} = 1 \text{ and } h_{ij} \leq -h_{\text{min}}, \\ 0, & \text{otherwise,} \end{cases} \quad (2)$$

such that only cells deeper than h_{min} (in absolute value) remain available. In this paper we mainly use $h_{\text{min}} = 20$ m as a conservative yet permissive value for large commercial vessels, and treat stricter depth constraints as a diagnostic in the Results.

2.3. Sea-ice dataset and regridding

Sea-ice concentration is taken from the CMEMS Arctic sea-ice reanalysis (Copernicus Marine Environment Monitoring Service, 2023), which provides daily fields of sea-ice concentration (SIC) and thickness on a polar stereographic grid for the Arctic Ocean and surrounding seas. We focus on the June–September 2018 season as a recent summer with complete CMEMS coverage and typical low Arctic sea-ice extent, rather than an extreme minimum year, so that the diagnostics reflect present-day conditions without being tied to an exceptional season.

The SIC variable (**siconc**) is expressed as fractional sea-ice concentration in $[0, 1]$. For each daily time step t_k we first subset the CMEMS product to a geographic box slightly larger than the routing domain and then regrid SIC onto the 0.5° routing grid via bilinear interpolation, yielding a time-dependent field $s_{ijk} \in [0, 1]$ on the same 89×399 grid as the bathymetry. Grid points south of the CMEMS ice domain (for which **siconc** is undefined) are assigned $s_{ijk} = 0$, consistent with the product being an Arctic sea-ice reanalysis.

The primary sea-ice control used in this study is a concentration threshold C_{thr} expressed as a fraction of ice cover (e.g. $C_{\text{thr}} = 0.15$ for 15% SIC). For a

given date t_k , we define an ice-feasibility mask

$$M_{ij}^{\text{ice}}(C_{\text{thr}}, t_k) = \begin{cases} 1, & M_{ij}^{\text{sea}} = 1 \text{ and } s_{ijk} < C_{\text{thr}}, \\ 0, & \text{otherwise,} \end{cases} \quad (3)$$

such that $M^{\text{ice}} = 1$ denotes ice-safe ocean at that date and threshold. The reference threshold used throughout is $C_{\text{thr}} = 0.15$ (15 % SIC), using a concentration threshold close to the WMO ‘open water’ category (total sea-ice concentration $< 1/10$; World Meteorological Organization (2014)); additional thresholds between 5 % and 50 % are used for sensitivity experiments.

2.4. Feasibility constraints: depth, ice and joint masks

All routing experiments are performed on binary feasibility masks that encode which cells are available to the pathfinding algorithm. We distinguish three types of masks:

1. **Sea-only mask** M^{sea} : this mask encodes pure geometric accessibility based on GEBCO bathymetry, with no additional safety constraints. It is used to construct a baseline “sea-only” route that avoids land but ignores both depth and sea-ice.
2. **Depth-constrained masks** $M^{\text{depth}}(h_{\min})$: these masks enforce under-keel clearance by excluding cells shallower than h_{\min} , as defined in Eq. (2). In practice we consider $h_{\min} = 20$ m as a realistic value for a deep-draught commercial vessel, and briefly explore stricter values ($h_{\min} = 50$ and 200 m) to assess how quickly trans-Arctic connectivity fragments at this resolution. To avoid artificially blocking port access, depth constraints may be relaxed in the immediate origin and destination cells while being enforced along the rest of the route.
3. **Ice-constrained masks** $M^{\text{ice}}(C_{\text{thr}}, t_k)$: these masks encode the subset of ocean cells that are both geometric sea and have SIC below a chosen threshold on date t_k , as defined in Eq. (3). They are used for seasonal and threshold sensitivity experiments in which only sea-ice is varied while bathymetry remains fixed.

For completeness we also define a *joint* depth-plus-ice mask

$$M_{ij}^{\text{joint}}(h_{\min}, C_{\text{thr}}, t_k) = M_{ij}^{\text{depth}}(h_{\min}) M_{ij}^{\text{ice}}(C_{\text{thr}}, t_k), \quad (4)$$

representing the intersection of depth and ice constraints. At the 0.5° resolution used here a continuous joint-safe corridor does not exist for $h_{\min} = 20$ m and $C_{\text{thr}} = 15\%$ in September 2018; this lack of connectivity is itself one of the diagnostics discussed in Section 3.4.1 and motivates the decision to treat bathymetry and sea-ice constraints separately in the main route analysis.

2.5. Graph construction and routing algorithm

Routing is performed on a regular-grid graph derived from the routing grid. Each ocean cell (i, j) with mask value $M_{ij} = 1$ (for the mask under consideration) is treated as a node. Undirected edges are added between each node and its von Neumann and diagonal neighbours (8-connectivity), provided that both endpoints are feasible ($M_{ij} = M_{i',j'} = 1$). The edge cost $c_{(i,j) \rightarrow (i',j')}$ is taken as the great-circle distance between the two cell centres, computed using a spherical Earth approximation with radius $R = 6371$ km; this ensures that the discrete cost field is consistent with physical distance.

Routes between a chosen origin and destination are computed using the A* algorithm. The heuristic $h(\cdot)$ is the great-circle distance from the current node to the destination, divided by a constant reference speed to preserve units; this heuristic is admissible and guarantees that A* returns a globally distance-minimising path on the graph. For masks that are purely geometric (sea-only) or purely ice-based, A* is therefore equivalent to finding the shortest feasible sea-only route in terms of travelled distance.

Throughout this paper we consider a canonical origin–destination (OD) pair chosen to span the pan-Arctic basin without tying the analysis to a specific port. The origin lies in the eastern North Atlantic at $(40.5^\circ \text{ N}, 19.5^\circ \text{ W})$, while the destination lies in the North Pacific at $(69.5^\circ \text{ N}, 179.5^\circ \text{ E})$. Both coordinates coincide with routing-grid cell centres and are located in the largest contiguous sea component under the pure bathymetric mask, so that a reference sea-only route exists. The great-circle distance between these points is approximately 4149 NM and serves as a lower bound against which gridded sea-only and constrained routes are compared.

2.6. Diagnostic metrics and experiment design

For each feasibility mask and OD pair we extract the A*-derived path as an ordered sequence of grid cells $\{(i_n, j_n)\}_{n=0}^{N-1}$, together with their geographic coordinates $(\varphi_{i_n}, \lambda_{j_n})$. From this discrete path we compute the following diagnostics:

- **Route distance** D_{route} : the sum of great-circle distances along each edge of the path, reported in nautical miles (NM).
- **Great-circle distance** D_{GC} : the great-circle distance between origin and destination, also in NM, representing the theoretical lower bound in the absence of land and safety constraints.
- **Route inflation** ρ : the ratio $D_{\text{route}}/D_{\text{GC}}$, which measures by how much the constrained route is elongated relative to the direct great-circle.
- **Depth statistics along the route**: for experiments that include bathymetric information we sample h_{ij} along the route and report the minimum, mean and maximum depths. In addition, one-dimensional profiles and histograms are used to compare the depth distribution along the route with that of all sea cells in the corridor.
- **Sea-ice statistics and connectivity**: for ice-constrained experiments we compute (i) the fraction of sea cells that are ice-safe ($M^{\text{ice}} = 1$), (ii) the number of connected components of the ice-safe sea, and (iii) whether the origin and destination lie in the same ice-safe component. These diagnostics are computed both for single dates and for seasonal sequences.

Two families of experiments are performed:

1. **Seasonal experiments**: for a fixed SIC threshold $C_{\text{thr}} = 0.15$ we evaluate ice-only routing on four representative summer dates (15 June, 15 July, 15 August and 15 September 2018). For each date we compute the fraction of ice-safe sea, the number of ice-safe components, and (if a route exists) the corresponding D_{route} and ρ .
2. **Threshold-sensitivity experiments**: for a late-summer date we vary the SIC threshold over $\{5, 10, 15, 30, 50\}$ % and repeat the diagnostics. A second experiment combines multiple dates (mid-June to end-September) and thresholds into a date–threshold matrix, from which we construct a heatmap of route availability and route inflation. Entries where no continuous ice-safe corridor exists are marked as missing, emphasising the discrete “opening” of the trans-Arctic connection in late summer.

Joint depth-plus-ice masks are analysed in a more qualitative way: for selected combinations of h_{\min} and C_{thr} we visualise the joint-safe sea fraction and its connected components, and record whether a continuous trans-Arctic corridor exists. At the 0.5° resolution considered here, no joint-safe path is found for $h_{\min} = 20$ m and $C_{\text{thr}} = 15\%$ in September 2018, highlighting the strong fragmentation induced by combining depth and ice constraints and motivating the separation of bathymetric and sea-ice effects in the present paper.

Notation for masks and thresholds

For convenience, Table 1 summarises the main symbols used for feasibility masks and thresholds in this paper.

Table 1: Notation for masks, fields and thresholds used in the routing framework.

Symbol	Type	Meaning
h_{ij}	scalar field	Water depth at routing-grid cell (i, j) from GEBCO 2024; negative over ocean, positive over land/ice.
M_{ij}^{sea}	binary mask	Static land/sea mask; $M_{ij}^{\text{sea}} = 1$ for ocean cells ($h_{ij} < 0$), 0 otherwise.
h_{\min}	parameter	Minimum acceptable water depth (under-keel clearance), e.g. 20 m, 50 m or 200 m.
$M_{ij}^{\text{depth}}(h_{\min})$	binary mask	Depth-safe sea mask; $M_{ij}^{\text{depth}} = 1$ if $M_{ij}^{\text{sea}} = 1$ and $h_{ij} \leq -h_{\min}$.
s_{ijk}	scalar field	Sea-ice concentration (SIC) at cell (i, j) and time index k regridded from CMEMS, in $[0, 1]$.
C_{thr}	parameter	SIC threshold for ice safety, expressed as fraction (e.g. 0.15 for 15%).
$M_{ij}^{\text{ice}}(C_{\text{thr}}, t_k)$	binary mask	Ice-safe sea mask at date t_k ; $M_{ij}^{\text{ice}} = 1$ if $M_{ij}^{\text{sea}} = 1$ and $s_{ijk} < C_{\text{thr}}$.
$M_{ij}^{\text{joint}}(h_{\min}, C_{\text{thr}}, t_k)$	binary mask	Joint depth-plus-ice mask; product of $M_{ij}^{\text{depth}}(h_{\min})$ and $M_{ij}^{\text{ice}}(C_{\text{thr}}, t_k)$.
D_{GC}	scalar	Great-circle distance between origin and destination (NM).
D_{route}	scalar	Distance of the A*-derived route on the grid (NM).
ρ	scalar	Route inflation factor, $\rho = D_{\text{route}}/D_{\text{GC}}$.

3. Results and Discussion

3.1. Bathymetric domain and baseline sea-only routing

We first define a static bathymetric routing grid for the trans-Arctic corridor. Bathymetry is taken from the GEBCO_2024 global grid and subset to the region 40–85°N and 20°W–180°E, which captures the North Atlantic, Barents and Kara seas, the Eurasian Arctic shelf and the Bering and North Pacific gateway. The native GEBCO field (15 arcsec) is coarsened to a regular $0.5^\circ \times 0.5^\circ$ latitude–longitude grid yielding a routing grid of 89×399 nodes (Fig. 1a). Within this domain, depths on the routing grid range from approximately -8700 m in the deep basins to $+5600$ m over land.

A binary land/sea mask is constructed by classifying grid cells with GEBCO elevation ≤ 0 m as sea and > 0 m as land (Fig. 1b). Connected-component labelling on the sea mask shows that the largest sea component forms a continuous oceanic corridor from the North Atlantic to the North Pacific across the Arctic, while smaller components correspond to enclosed shelf seas and fjords. This mask defines the static sea-only feasibility constraint used throughout the remainder of the study.

To obtain a canonical baseline route, we consider an idealised trans-Arctic origin–destination (OD) pair between a North Atlantic waypoint at (40.5°N, 19.5°W) and a North Pacific waypoint at (69.5°N, 179.5°E), corresponding to the south-western and north-eastern corners of the routing domain. The great-circle distance between these two waypoints is 4149.6 NM. Routing on the 0.5° grid is performed using an A* search with edge costs equal to the great-circle distance between neighbouring grid nodes, restricted to cells in the static sea mask. The resulting sea-only route is shown in Fig. 2 and runs northwards out of the North Atlantic, skirts the Eurasian Arctic shelf break and exits into the North Pacific.

The sea-only route distance is 4561.1 NM, i.e. approximately 10% longer than the unconstrained great-circle distance. At a design speed of 14 kn this corresponds to a travel time of 13.6 days, compared to 12.4 days for the great-circle, implying a penalty of about 1.2 days purely due to enforcing sea-only feasibility on a coarse grid. Bathymetry sampled along the route (Fig. 3) indicates that the path remains predominantly in deep water: depths along the route have a mean of ≈ -3300 m, with a minimum of ≈ -5700 m and a shallowest segment of ≈ -30 m. The associated depth histogram shows that the route samples the deeper part of the corridor-wide depth distribution, with only a few segments approaching the continental shelf.

This confirms that the purely geometric sea-only constraint already tends to select deep-water pathways, even before any explicit bathymetric safety threshold is applied.

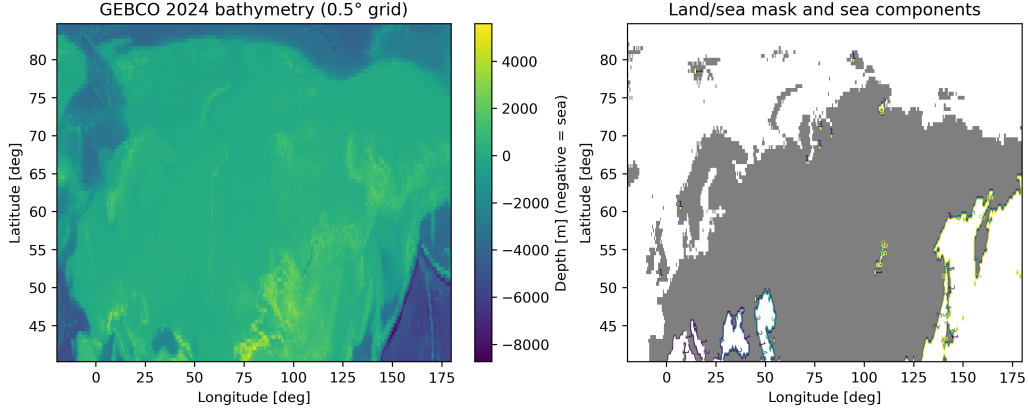


Figure 1: (a) GEBCO 2024 bathymetry coarsened to a $0.5^\circ \times 0.5^\circ$ routing grid over the Arctic corridor (40–85°N, 20°W–180°E). (b) Derived land/sea mask and connected sea components; the largest sea component links the North Atlantic and North Pacific, while smaller ones are enclosed shelf seas and fjords.

3.2. Bathymetric safety thresholds and routing connectivity

Having established a purely geometric sea-only route on the GEBCO-based grid, we next examine how explicit bathymetric safety thresholds affect network connectivity and route geometry. For a given minimum safe depth h_{\min} , the depth-safe sea mask $M_{ij}^{\text{depth}}(h_{\min})$ is defined in Eq. (2) as taking the value 1 where cell (i, j) is ocean and $h_{ij} \leq -h_{\min}$, and 0 otherwise; that is, only grid cells deeper than h_{\min} are considered navigable.

In practice we apply this threshold to all interior cells of a candidate route, while allowing the origin and destination cells themselves to be shallower (“endpoints relaxed”), mimicking the fact that vessels typically enter or leave deep-water routes through local port approaches.

On the 0.5° routing grid, the static sea mask occupies approximately 48% of all cells. Imposing a relatively mild depth constraint of $h_{\min} = 20$ m retains 94% of this sea area as depth-safe ($\approx 45\%$ of the whole grid) and leaves the canonical trans-Arctic origin and destination in the same connected component. Running A* on this depth-safe mask yields a route that is effectively identical to the baseline sea-only path: the distance remains

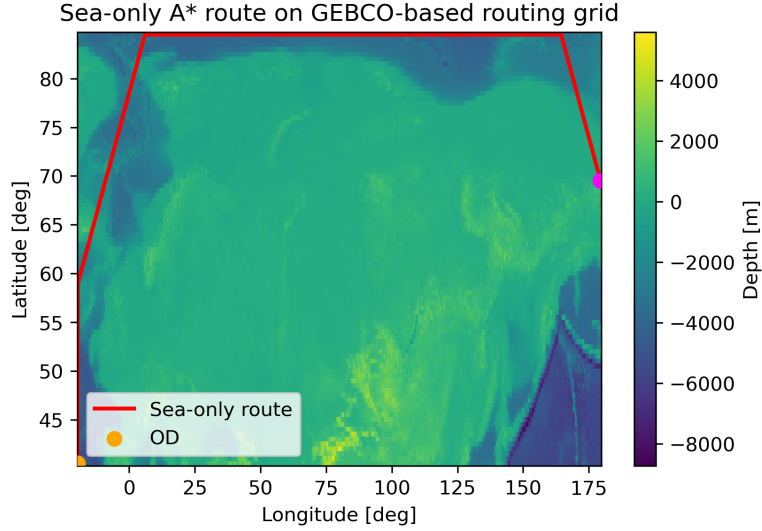


Figure 2: Sea-only A* route (red) between the canonical origin–destination pair overlaid on the GEBCO-based 0.5° bathymetry. The route remains within the static sea mask and follows deep-water pathways along the Arctic margin.

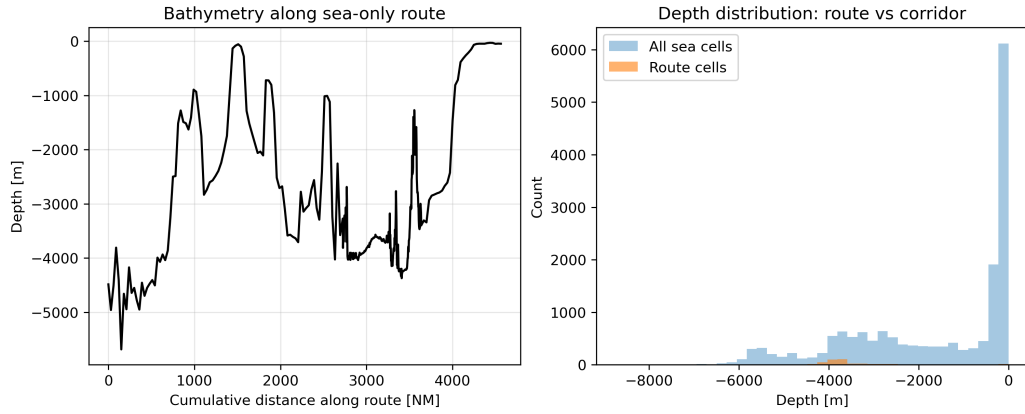


Figure 3: (a) Bathymetry along the baseline sea-only route as a function of cumulative distance. (b) Depth histograms for all sea cells in the corridor (blue) and for routed cells (orange); the route samples predominantly deep water and only briefly crosses shallow shelves.

4561 NM, corresponding to a 10% inflation over the great-circle distance, and depths sampled along the route remain almost entirely in deep water (Fig. 4, cf. Fig. 3). This confirms that, at the scale of our corridor, the unconstrained sea-only route already follows the deep-ocean backbone and does not exploit marginally shallow shortcuts.

As the minimum safe depth is tightened, the navigable network gradually fragments. For $h_{\min} = 50$ m, only about 85% of the original sea area remains depth-safe; by $h_{\min} = 200$ m this drops to roughly two-thirds of the sea mask. The number of depth-safe connected components increases from 30 to more than 35 as the threshold is raised, and beyond $h_{\min} \approx 50$ m the canonical origin and destination lie in different depth-safe components (Fig. 5b). In other words, at this resolution there is no continuous path between the Atlantic and Pacific gateways that is everywhere deeper than 50–200 m.

The spatial pattern of these constraints is illustrated in Fig. 4a, where the sea-only route is overlaid on bathymetry with selected isobaths. Narrow shallow features along the shelf break and in straits appear as “choke points” that disconnect the deep-water network once a stringent depth threshold is enforced. From an operational perspective, vessels with realistic draughts could still transit these regions, but at the 0.5° grid spacing they collapse into single grid cells that are either fully safe or fully blocked. This highlights an important trade-off: coarser grids are computationally attractive for large-scale scenario analysis, but they can overstate the impact of bathymetric constraints in narrow passages.

A complementary diagnostic is provided by the depth distribution in the corridor versus along the route (Fig. 3). While the overall sea area spans depths from approximately -100 to -6000 m, the A* route samples predominantly the deeper part of this distribution, with a long tail towards abyssal depths and only a small fraction of cells shallower than 100 m. Together with the connectivity analysis, this suggests that in the present configuration bathymetry is *not* the primary limiting factor for a trans-Arctic corridor at the coarse planning scale; rather, the static sea-only feasibility and the seasonal sea-ice field (addressed in the following sections) are the dominant controls on route availability.

3.3. Seasonal opening of an ice-safe trans-Arctic corridor

We now investigate how seasonal sea-ice concentration modulates the feasibility and geometry of the trans-Arctic corridor on the static bathymetric grid. Sea-ice concentration (SIC) is taken from the CMEMS Arctic sea-ice

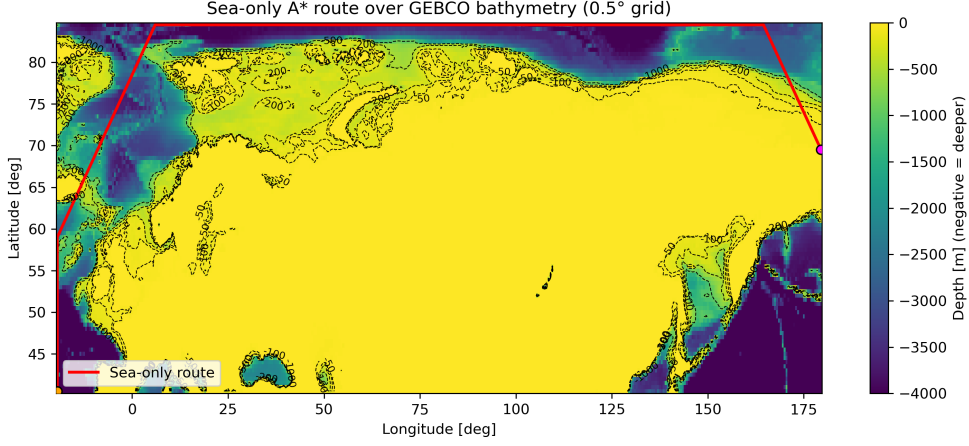


Figure 4: Sea-only A* route (red) over GEBCO 2024 bathymetry on the 0.5° grid, with selected isobaths. The path tracks the Arctic shelf break and remains mostly in deep water even without explicit depth constraints.

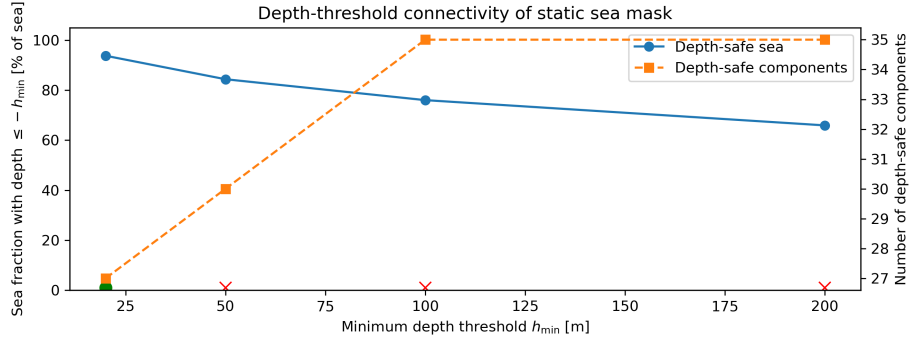


Figure 5: Effect of minimum depth h_{\min} on the fraction of depth-safe sea area (blue, left axis) and the number of depth-safe components (orange, right axis). Markers indicate whether the canonical origin and destination lie in the same component (route possible) or not.

reanalysis for June–September 2018 and regridded onto the 0.5° routing grid by bilinear interpolation. For each target date we extract the nearest model time, apply a fixed ice-safety criterion of $\text{SIC} < 15\%$, and intersect this ice-safe mask with the static sea mask. The resulting ice-safe sea area and associated connectivity are then evaluated for the canonical origin–destination pair.

Figure 6 shows the evolution of the ice-safe sea fraction between mid-June and mid-September 2018, expressed as a percentage of the static sea mask. In mid-June (15 June), only 58.6% of the sea area is ice-safe under the $\text{SIC} < 15\%$ criterion and the ice-safe domain is fragmented into 96 disconnected components. By mid-July the ice-safe fraction has increased to 65.5% and the number of components has decreased to 66, but no continuous ice-safe path exists between the Atlantic and Pacific gateways. A qualitatively different regime emerges in late summer: by 15 August, 77.0% of the sea area is ice-safe and the number of components has dropped to 33, at which point the canonical origin and destination first fall within the same ice-safe component. By 15 September the ice-safe fraction reaches 80.7% of the static sea mask, still partitioned into 33 components, but with a robust large-scale path spanning the Arctic. These seasonal changes in ice-safe area, connectivity and route availability are summarised in Table 2.

Table 2: Seasonal evolution of ice-safe sea area and route availability for the canonical trans-Arctic origin–destination pair under the $\text{SIC} < 15\%$ criterion. Ice-safe fractions are expressed relative to the static sea mask. “Route” indicates whether a continuous ice-safe path exists.

Date (2018)	Ice-safe sea [% of sea]	Ice-safe components	Route	D_{route} [NM]	$\rho = D_{\text{route}}/D_{\text{GC}}$
15 June	58.6	96	No	–	–
15 July	65.5	66	No	–	–
15 August	77.0	33	Yes	5206.0	1.255
15 September	80.7	33	Yes	5019.9	1.210

The impact of this seasonal evolution on routing is summarised in Fig. 7. For the early-summer dates (15 June and 15 July) no ice-safe route exists under the $\text{SIC} < 15\%$ threshold, i.e. the trans-Arctic corridor is effectively *closed* for the chosen origin–destination pair despite the existence of a deep-water backbone. From 15 August onwards, an ice-safe sea-only route becomes available. On 15 August its length is 5206 NM, corresponding to a route-to-great-circle ratio of 1.255; by 15 September the distance has shortened to 5019.9 NM and the ratio to 1.210. For comparison, the static bathymetry-

based sea-only route (ignoring ice) is 4561.1 NM with a ratio of 1.099 relative to the 4149.6 NM great-circle distance. Thus, even once the corridor is open in late summer, the ice-safe route remains approximately 10% longer than the static sea-only path and about 20–25% longer than the great-circle.

An illustrative late-summer ice-feasibility map and corresponding shortest route are shown in Fig. 8 for 15 September 2018. In mid-August, residual ice in the central Arctic and along parts of the Siberian margin forces the route to skirt the ice edge, yielding a strongly curved path that stays close to the deep Norwegian–Greenland Sea and the Pacific side of the Arctic basin. By mid-September, the ice extent has retreated further towards the central Arctic and the marginal seas are largely accessible, allowing the route to cut more directly across the basin and shorten by almost 200 NM. Despite this shortening, the corridor remains substantially longer than both the bathymetry-only path and the unconstrained great-circle.

Taken together, these results highlight that for a given bathymetric grid the presence of sea ice imposes a *binary* control on trans-Arctic feasibility at seasonal timescales. For early-summer conditions in 2018 the chosen origin–destination pair cannot be connected by any continuous ice-safe path under a conservative $\text{SIC} < 15\%$ threshold, even though a deep-water backbone exists. Once the corridor opens in late summer, sea-ice still adds a second-order but non-negligible distance penalty on top of the static sea-only inflation. This suggests that, from the perspective of large-scale voyage planning, the timing of the seasonal ice retreat is a more critical driver of trans-Arctic feasibility than moderate variations in the exact ice-safety threshold, an aspect further explored in the threshold-sensitivity analysis in Section 3.4.

3.4. Sensitivity to the ice-safety threshold

The previous section adopted a conservative but conventional ice-safety criterion of $\text{SIC} < 15\%$ to define navigable sea. Here we examine how sensitive the large-scale routing results are to this choice by varying the threshold over a broad range of values and repeating the analysis.

We first fix the date to 15 September 2018, when the canonical origin–destination pair is connected by an ice-safe route for the reference threshold, and vary the ice-safety cut-off across $\text{SIC} < 5\%$, 10% , 15% , 30% and 50% . For each threshold we recompute the fraction of static sea area that is ice-safe, the number of disconnected ice-safe components, and, where possible, the shortest ice-safe A* route between the Atlantic and Pacific gateways. As shown in Fig. 9, the ice-safe area fraction increases only modestly across this

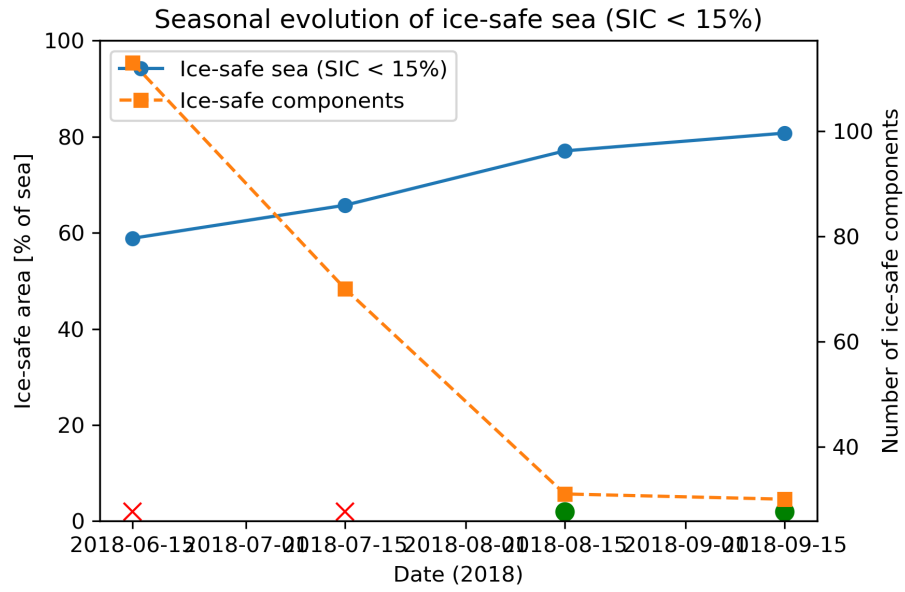


Figure 6: Seasonal evolution of the ice-safe sea fraction (blue, left axis) and number of ice-safe components (orange, right axis) for SIC < 15%. Markers show dates when the canonical origin and destination lie in the same ice-safe component (route exists) or not.

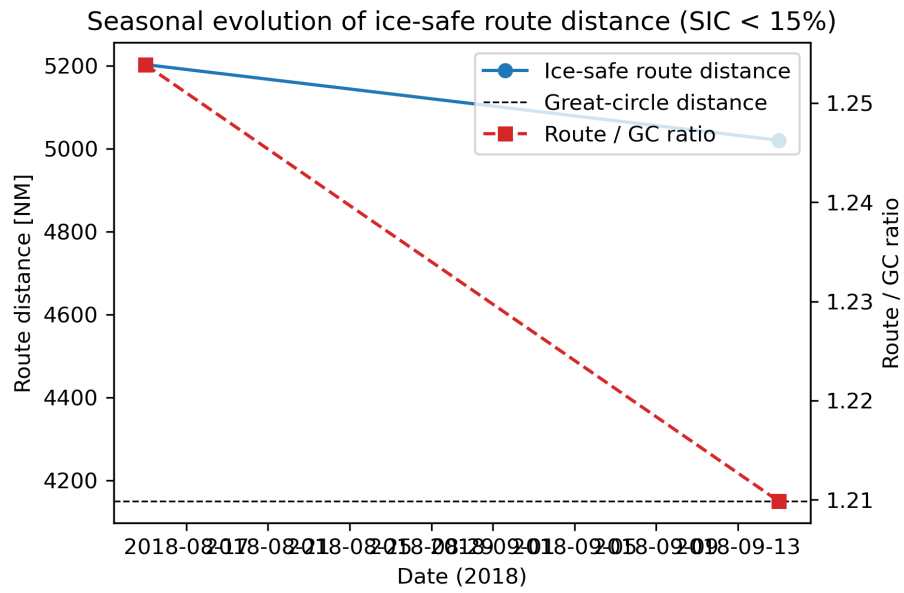


Figure 7: Seasonal evolution of the shortest ice-safe route distance (circles, left axis) and route-to-great-circle ratio (red dashed line, right axis) for SIC < 15%. No route exists in June and mid-July; from mid-August the corridor opens and gradually shortens as ice retreats.

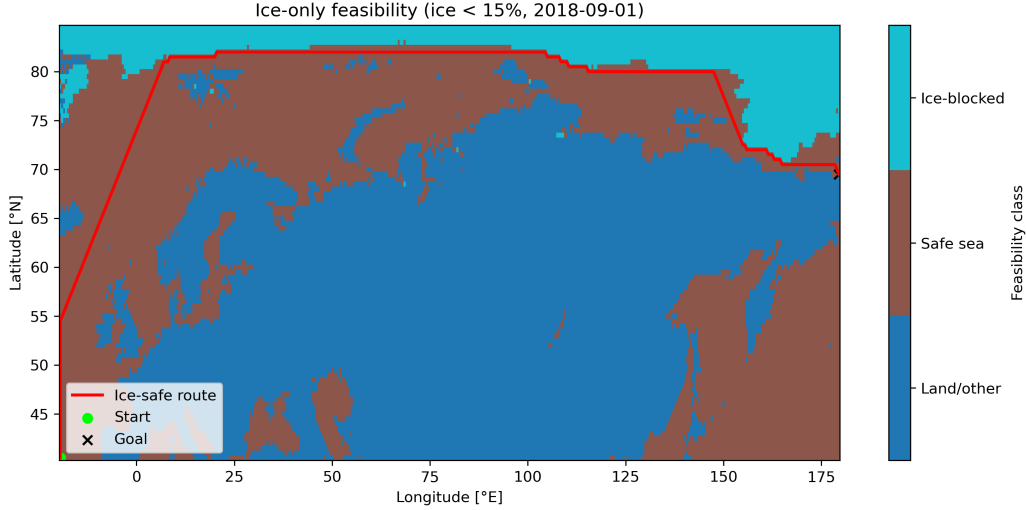


Figure 8: Ice-only feasibility on 15 September 2018 for the canonical origin–destination pair under the $\text{SIC} < 15\%$ criterion. Brown shading shows ice-safe sea, cyan shows sea blocked by ice, and blue indicates land or non-sea. The red line is the shortest ice-safe route, with origin and destination marked.

range, from approximately 80.4% of the sea mask at $\text{SIC} < 5\%$ to 81.5% at $\text{SIC} < 50\%$. The number of ice-safe components fluctuates between roughly 33 and 44, reflecting local changes in the connectivity of marginal-ice zones, but the canonical origin and destination remain in the same ice-safe component for all thresholds considered.

The resulting route distances are remarkably insensitive to the choice of threshold. For 15 September 2018, the shortest ice-safe sea-only path ranges from 5024.5 NM at $\text{SIC} < 5\%$ to 5018.6 NM at $\text{SIC} < 50\%$, corresponding to route-to-great-circle ratios between 1.211 and 1.209. This spread of less than 6 NM and $< 0.2\%$ in ratio is negligible compared to the $\approx 10\%$ inflation relative to the bathymetry-only sea route and the $\approx 20\%$ inflation relative to the unconstrained great-circle distance. In other words, once the large-scale trans-Arctic corridor is open, moderate tightening or relaxation of the ice-safety threshold within the range 5–50% has only a second-order effect on route length.

To place this in a broader seasonal context, we extend the analysis to a grid of dates and thresholds. For a set of representative dates between 15 June 2018 and 30 September 2018, and for each of the five thresholds, we recompute the ice-safe mask and attempt to route the canonical origin–

destination pair. The resulting route-to-great-circle ratios are summarised in Fig. 10. Early in the season (mid-June and early July), no continuous ice-safe path exists for any of the thresholds in the 5–50% range: the canonical gateways lie either outside the ice-safe domain or in different disconnected components. The corridor thus remains effectively closed, independently of the exact choice of SIC cut-off.

A qualitatively different regime emerges once the seasonal ice cover retreats sufficiently. From mid-August onwards, an ice-safe trans-Arctic route exists for all tested thresholds, with route-to-great-circle ratios between ≈ 1.25 and ≈ 1.20 . The dominant gradient in the heatmap is along the *time* axis: ratios decrease from about 1.25 in mid-August to about 1.20 by late September as the corridor widens and routes can cut more directly across the basin. In contrast, variation along the threshold axis at a given date is weak, typically at the level of a few tenths of a percent in route length.

These results reinforce the interpretation that, at the scale of the present corridor and grid, the seasonal timing of the ice retreat exerts a first-order control on route feasibility and length, while the precise value of the ice-safety threshold within a reasonable range primarily influences local connectivity and the detailed shape of marginal-ice detours. For the purposes of large-scale historical route diagnostics, a single reference threshold such as $\text{SIC} < 15\%$ therefore appears adequate, provided that the associated limitations for narrow passages and coastal approaches are made explicit.

3.4.1. Joint bathymetric and ice constraints

The previous subsections considered bathymetric and ice constraints separately. In a final diagnostic step we combined both into a joint feasibility mask, requiring each routing cell to be (i) ocean, (ii) deeper than a minimum under-keel clearance threshold h_{\min} , and (iii) ice-safe in the sense that sea-ice concentration (SIC) remains below a navigational limit c_{ice}^{\max} . Here we adopt $h_{\min} = 20$ m and $c_{\text{ice}}^{\max} = 15\%$ as representative values for unrestricted open-water vessels and commonly used SIC thresholds in Arctic route screening.

For a late-summer snapshot (15 September 2018) the routing grid sea fraction can be decomposed as follows. Using only bathymetry, 93.8% of the sea cells are deeper than 20 m, confirming that depth alone is not a primary limiting factor at the 0.5° corridor scale. Using only ice, 80.8% of sea cells satisfy $\text{SIC} < 15\%$ on that date. When both constraints are applied simultaneously, the fraction of *joint-safe* sea decreases to 74.6% of the sea mask. While this reduction in area is modest, its spatial organisation changes

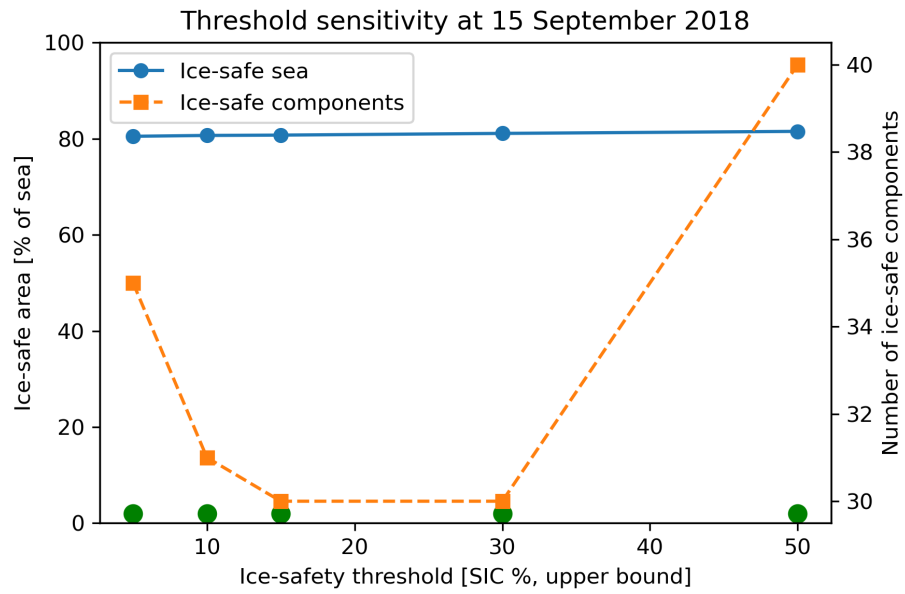


Figure 9: Sensitivity of ice-safe routing to the SIC threshold on 15 September 2018: fraction of ice-safe sea (blue, left axis), number of ice-safe components (orange, right axis), and OD connectivity (markers).

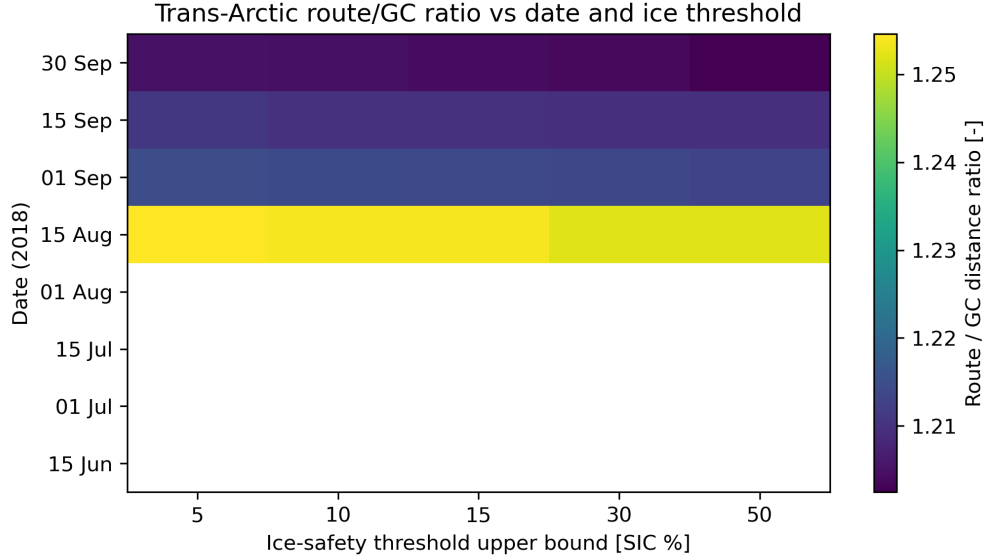


Figure 10: Route-to-great-circle distance ratio for the canonical origin–destination pair as a function of date and SIC threshold. Colours show ratios for the shortest ice-safe routes; white crosses indicate combinations with no continuous ice-safe path.

markedly: the joint-safe mask is split into 35 disconnected components on the 0.5° grid.

Figure 11 shows the resulting classification of the Arctic corridor into land, sea blocked by either depth or ice, and joint-safe sea. The canonical trans-Arctic OD endpoints lie in different joint-safe components (labels 1 and 20), so that no continuous route exists that simultaneously respects $h_{\min} = 20$ m and $\text{SIC} < 15\%$ along the entire path. This is in stark contrast to the sea-only and ice-only experiments, where late-summer Atlantic–Pacific connections could still be traced across the same grid Table 3.

These results highlight that, even in a relatively favourable ice year such as 2018, the combination of shallow shelves and residual marginal ice is capable of severing trans-Arctic connectivity at coarse resolution for realistic under-keel and SIC thresholds. In other words, large-scale bathymetry-conditioned, ice-only route diagnostics (Sections 3.2 and 3.3) are optimistic upper bounds on what can be achieved when both constraints are enforced simultaneously. From an operational perspective this supports a two-step interpretation: (i) the present paper’s sea-only and ice-only corridors provide an envelope of *where* and *when* an Arctic route might be attractive

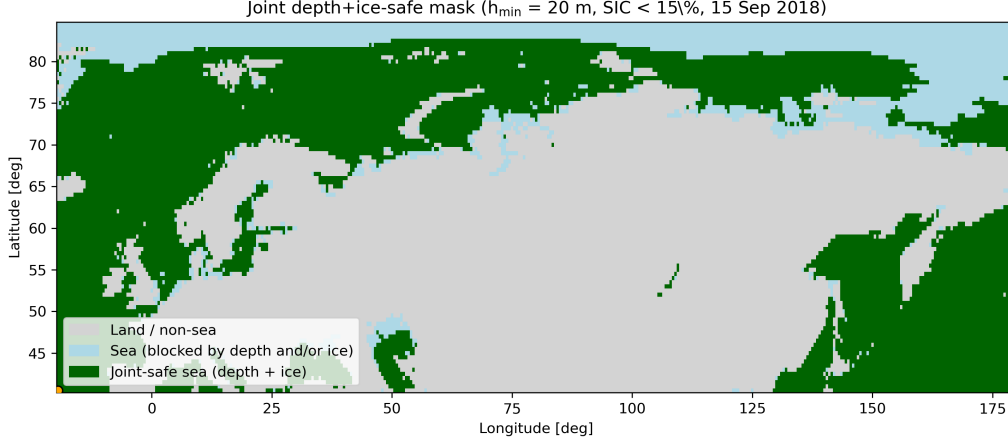


Figure 11: Joint depth–ice feasibility mask ($h \geq 20$ m, $\text{SIC} < 15\%$) on the 0.5° routing grid for 15 September 2018. Land, blocked sea and joint-safe sea are shown; the canonical origin and destination lie in different joint-safe components, so no continuous depth- and ice-safe route exists.

at the basin scale, while (ii) realistic planning for specific vessels and ports will require higher-resolution bathymetry and sea-ice information, which we address in subsequent work.

3.4.2. Summary of key implications for large-scale Arctic route diagnostics

The experiments in Sections 3.1–3.4.1 allow a number of robust conclusions about large-scale Arctic route diagnostics on a fixed geographic grid. To provide context for these conclusions, Table 3 summarises the canonical trans-Arctic route distance and inflation factor under the main constraint combinations considered in this study.

Table 3: Canonical trans-Arctic route distances and inflation factors under different constraint sets. D_{GC} is the great-circle distance between origin and destination; D_{route} is the A*-derived path length on the routing grid; $\rho = D_{\text{route}}/D_{\text{GC}}$.

Scenario	D_{route} [NM]	ρ	Notes
Great-circle (unconstrained)	4149.6	1.000	Theoretical lower bound
Sea-only (GEBCO, static)	4561.1	1.099	Land mask only; no ice or depth constraints
Ice-only, 15 August 2018 ($\text{SIC} < 15\%$)	5206.0	1.255	First date with continuous ice-safe corridor
Ice-only, 15 September 2018 ($\text{SIC} < 15\%$)	5019.9	1.210	Late-summer minimum of ice-constrained distance
Joint depth+ice, 15 September 2018 ($h_{\min} = 20$ m, $\text{SIC} < 15\%$)	–	–	No continuous joint-safe route

First, enforcing sea-only feasibility on GEBCO 2024 already lengthens the canonical trans-Arctic connection by about 10% relative to a great-circle,

even before any environmental constraints are applied. This confirms that widely used rule-of-thumb shortcuts for trans-Arctic corridors underestimate path length once sharp coastlines and islands are honoured on a realistic bathymetric grid.

Second, depth constraints at 0.5° resolution are relatively benign for open-ocean routing. For representative under-keel limits of $h_{\min} = 20\text{--}50$ m, more than 85% of the sea mask remains depth-safe, and a sea-only route persists for $h_{\min} = 20$ m. Bathymetry therefore acts primarily as a static structural constraint, shaping the corridor but not fundamentally blocking the basin-scale connection at this resolution.

Third, historical sea-ice concentration is the dominant time-varying control on trans-Arctic connectivity in the present framework. The fraction of ice-safe sea ($\text{SIC} < 15\%$) increases from roughly 60% in mid-June to over 80% in mid-September, and a continuous trans-Arctic ice corridor only appears from mid-August onwards. Once open, the resulting ice-constrained routes are systematically longer than the sea-only benchmark, but their excess distance decreases by about 200 NM between August and late September as the marginal ice zone retreats.

Fourth, at the large scales considered here the existence and length of an ice-constrained route are only weakly sensitive to the exact SIC threshold in the range 5–50%. Changing the threshold modifies the fraction of ice-safe sea by a few percentage points but only perturbs route length by $\sim 20\text{--}30$ NM when a route exists. For basin-scale diagnostics this suggests that the choice of SIC threshold is less critical than the choice of season and year, although it will matter more once finer grids and coastal passages are resolved.

Finally, combining bathymetry and ice into a joint feasibility mask reveals that even a relatively mild under-keel constraint ($h_{\min} = 20$ m) can fragment the apparently open late-summer ice corridor. On 15 September 2018, only 74.6% of sea cells satisfy both depth and SIC criteria simultaneously, split into 35 disconnected components, and the canonical origin and destination fall into different components. At 0.5° resolution there is therefore no continuous route that is simultaneously sea-only, depth-safe and ice-safe along its full length.

Taken together, these results position the present study as a basin-scale, *offline* screening tool: it quantifies how static bathymetry and historical ice fields shape the feasibility and excess distance of trans-Arctic routes, and delineates the temporal window during which such connections are even theoretically possible. In the companion work we build on this foundation

by moving to time-evolving forecasts, finer grids and multi-objective cost functions better aligned with operational routing practice.

4. Conclusions

This study developed an offline, grid-based framework for diagnosing the feasibility and geometry of trans-Arctic shipping routes under static bathymetric and historical sea-ice constraints. Using GEBCO 2024 bathymetry re-gridded to a 0.5° pan-Arctic corridor ($40\text{--}85^\circ\text{N}$, $20^\circ\text{W}\text{--}180^\circ\text{E}$), we constructed a sea-only routing mask and applied A* search to a canonical west–east origin–destination pair. Even without environmental forcing, enforcing strict sea-only feasibility increased route length from 4,150 NM (great-circle) to about 4,560 NM (sea-only), i.e. a $\sim 10\%$ penalty arising purely from the shape of coastlines and islands on a realistic bathymetric grid.

Static depth constraints at 0.5° resolution were found to be relatively benign at basin scale. For representative under-keel limits of $h_{\min} = 20\text{--}50$ m, more than 85% of the sea mask remained depth-safe, and a sea-only route persisted for $h_{\min} = 20$ m. Depth therefore acts as a structural constraint—eliminating shallow shelves and passages—but does not, by itself, prevent large-scale trans-Arctic connectivity in this configuration. Bathymetry still matters, however, for shaping where such routes can run and for interpreting how close candidate paths approach shallow and coastal zones.

Historical sea-ice concentration emerged as the dominant time-varying control. Using summer 2018 CMEMS sea-ice concentration re-gridded to the same 0.5° routing grid and an ice-safety threshold of $\text{SIC} < 15\%$, the fraction of ice-safe sea increased from roughly 60% in mid-June to over 80% in mid-September. Continuous ice-safe trans-Arctic routes appeared only from mid-August onwards and were consistently longer than the sea-only benchmark: $\sim 5,200$ NM in mid-August, decreasing to $\sim 5,000$ NM by late September as the marginal ice zone retreated. The excess-distance penalty relative to great-circle therefore drops from about 25% to 20% over this late-summer window, highlighting how the timing of Arctic transits trades off against both feasibility and path length.

At the large scales considered here, route geometry was only weakly sensitive to the precise sea-ice threshold once a route existed. Varying the concentration threshold between 5 and 50% changed the fraction of ice-safe sea by a few percentage points and altered route length by only 20–30 NM. For coarse-grid, basin-scale diagnostics this suggests that the choice of SIC

threshold is less critical than the choice of season and year, although the threshold will become more important once narrower passages and coastal traffic lanes are resolved.

Combining bathymetry and ice into a joint feasibility mask exposed a more restrictive picture. For a relatively mild depth constraint ($h_{\min} = 20$ m) and $\text{SIC} < 15\%$ on 15 September 2018, only about 75% of sea cells were simultaneously depth-safe and ice-safe, split into 35 disconnected components. In this joint mask the canonical origin and destination fall into different components, and no fully depth- and ice-safe trans-Arctic route exists at 0.5° resolution. This underlines that optimistic statements about a “seasonally ice-free” Arctic can overstate actual navigable connectivity once realistic draft constraints are imposed.

The present framework has several limitations that also point directly to future work. First, the routing grid is coarse ($0.5^\circ \approx 55$ km), so narrow straits, detailed coastline geometry and port approaches are not resolved; the results are intended as basin-scale diagnostics, not operational tracks. Second, only a single canonical origin–destination pair and a single summer season (2018) were analysed; extending the analysis to a portfolio of Europe–Asia and intra-Arctic ODs and to multi-year sea-ice statistics would better capture inter-annual variability. Third, cost was defined purely as geographic distance, without explicit representation of metocean forcing, resistance, fuel consumption, emissions, or risk. Finally, several safety-relevant factors—sea-ice thickness, ridging, traffic separation schemes, and region-specific regulatory corridors—are omitted and should be incorporated before any operational use.

Despite these limitations, the study provides a physically grounded baseline for large-scale, safety-constrained Arctic routing. It quantifies how static bathymetry and historical sea ice jointly shape the feasibility, timing and excess distance of trans-Arctic connections, and it delineates when such routes are even theoretically open. Follow-on work will build directly on this foundation by (i) increasing spatial resolution and adding multiple ODs, (ii) integrating time-evolving sea-ice forecasts and metocean forcing into dynamic cost fields, and (iii) extending the single-distance metric towards multi-objective formulations that link routing more directly to fuel consumption, emissions and schedule reliability.

CRediT authorship contribution statement

Abdella Mohamed: Conceptualization, Methodology, Coding, Data curation, Writing, Visualization, Investigation, Validation. **Xiangyu Hu:** Supervision, Conceptualization, Methodology, Manuscript review and editing.

Acknowledgements

This work was supported by Technical University of Munich and Everlence (formerly: MAN Energy Solutions).

Data and Code Availability

Bathymetry data are taken from the GEBCO 2024 global grid (GEBCO Bathymetric Compilation Group, 2024), available at <https://www.gebco.net/>. Sea-ice concentration fields are taken from the CMEMS Arctic Ocean Sea Ice Reanalysis (Copernicus Marine Environment Monitoring Service, 2023), available via doi:10.48670/mds-00336.

The Python code used to construct feasibility masks and perform A* routing, together with configuration files specifying all parameters used in this study, is openly available at <https://doi.org/10.5281/zenodo.17863887>, under an open-source licence.

Declaration of Generative AI and AI-assisted Technologies in the Preparation of this Work

The authors used OpenAI ChatGPT to assist with language editing during manuscript preparation. The authors reviewed and edited all AI-generated content and take full responsibility for the scientific integrity and accuracy of the manuscript.

List of Tables

1	Notation for masks, fields and thresholds used in the routing framework.	12
---	--	----

2	Seasonal evolution of ice-safe sea area and route availability for the canonical trans-Arctic origin–destination pair under the SIC < 15% criterion. Ice-safe fractions are expressed relative to the static sea mask. “Route” indicates whether a continuous ice-safe path exists.	18
3	Canonical trans-Arctic route distances and inflation factors under different constraint sets. D_{GC} is the great-circle distance between origin and destination; D_{route} is the A*-derived path length on the routing grid; $\rho = D_{route}/D_{GC}$	26

List of Figures

1	(a) GEBCO 2024 bathymetry coarsened to a $0.5^\circ \times 0.5^\circ$ routing grid over the Arctic corridor (40–85°N, 20°W–180°E). (b) Derived land/sea mask and connected sea components; the largest sea component links the North Atlantic and North Pacific, while smaller ones are enclosed shelf seas and fjords. . . .	14
2	Sea-only A* route (red) between the canonical origin–destination pair overlaid on the GEBCO-based 0.5° bathymetry. The route remains within the static sea mask and follows deep-water pathways along the Arctic margin.	15
3	(a) Bathymetry along the baseline sea-only route as a function of cumulative distance. (b) Depth histograms for all sea cells in the corridor (blue) and for routed cells (orange); the route samples predominantly deep water and only briefly crosses shallow shelves.	15
4	Sea-only A* route (red) over GEBCO 2024 bathymetry on the 0.5° grid, with selected isobaths. The path tracks the Arctic shelf break and remains mostly in deep water even without explicit depth constraints.	17
5	Effect of minimum depth h_{min} on the fraction of depth-safe sea area (blue, left axis) and the number of depth-safe components (orange, right axis). Markers indicate whether the canonical origin and destination lie in the same component (route possible) or not.	17

6	Seasonal evolution of the ice-safe sea fraction (blue, left axis) and number of ice-safe components (orange, right axis) for $SIC < 15\%$. Markers show dates when the canonical origin and destination lie in the same ice-safe component (route exists) or not.	20
7	Seasonal evolution of the shortest ice-safe route distance (circles, left axis) and route-to-great-circle ratio (red dashed line, right axis) for $SIC < 15\%$. No route exists in June and mid-July; from mid-August the corridor opens and gradually shortens as ice retreats.	21
8	Ice-only feasibility on 15 September 2018 for the canonical origin–destination pair under the $SIC < 15\%$ criterion. Brown shading shows ice-safe sea, cyan shows sea blocked by ice, and blue indicates land or non-sea. The red line is the shortest ice-safe route, with origin and destination marked.	22
9	Sensitivity of ice-safe routing to the SIC threshold on 15 September 2018: fraction of ice-safe sea (blue, left axis), number of ice-safe components (orange, right axis), and OD connectivity (markers).	24
10	Route-to-great-circle distance ratio for the canonical origin–destination pair as a function of date and SIC threshold. Colours show ratios for the shortest ice-safe routes; white crosses indicate combinations with no continuous ice-safe path.	25
11	Joint depth–ice feasibility mask ($h \geq 20$ m, $SIC < 15\%$) on the 0.5° routing grid for 15 September 2018. Land, blocked sea and joint-safe sea are shown; the canonical origin and destination lie in different joint-safe components, so no continuous depth- and ice-safe route exists.	26
A1	GEBCO 2024 land/sea mask highlighting the Arctic routing domain ($40\text{--}85^\circ\text{N}$, $20^\circ\text{W}\text{--}180^\circ\text{E}$) in the global context.	33
A2	Shallow sea areas shallower than 50 m (red circles) over GEBCO 2024 bathymetry on the 0.5° routing grid, together with the canonical trans-Arctic sea-only route.	34
A3	Sensitivity of late-summer (15 September 2018) trans-Arctic route distance to the choice of ice-safety threshold. Solid line: ice-constrained route; dashed line: bathymetry-only sea route; dotted line: great-circle distance.	34

Appendix A. Supplementary figures

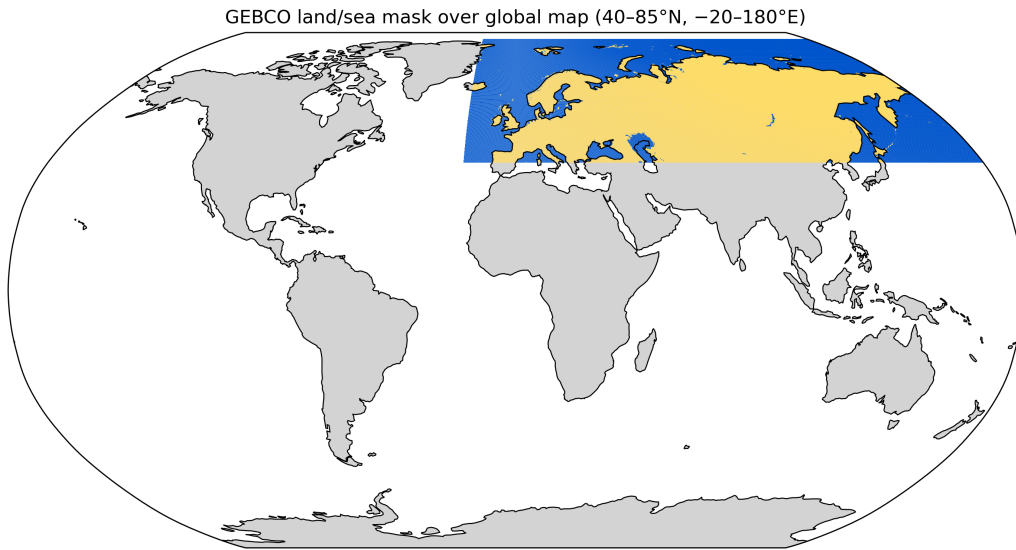


Figure A1: GEBCO 2024 land/sea mask highlighting the Arctic routing domain (40–85°N, 20°W–180°E) in the global context.

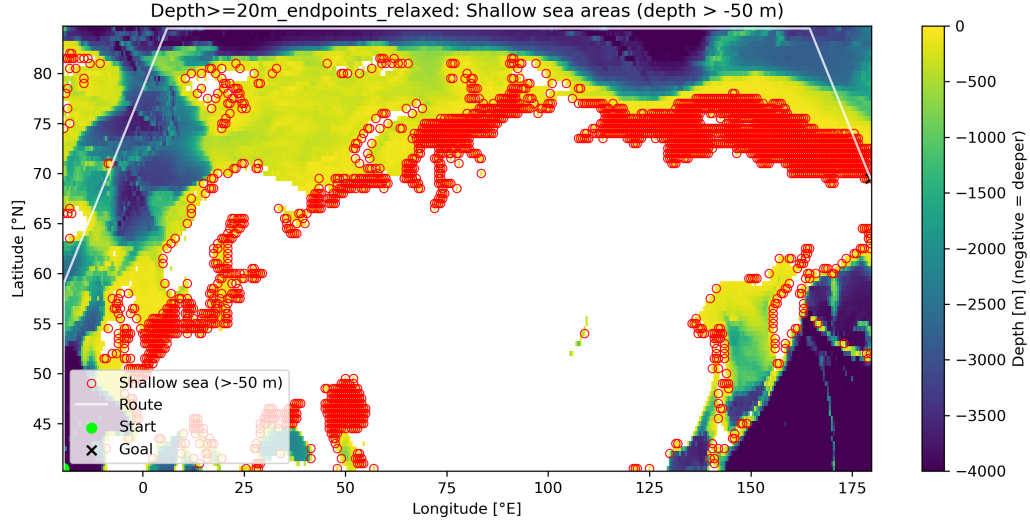


Figure A2: Shallow sea areas shallower than 50 m (red circles) over GEBCO 2024 bathymetry on the 0.5° routing grid, together with the canonical trans-Arctic sea-only route.

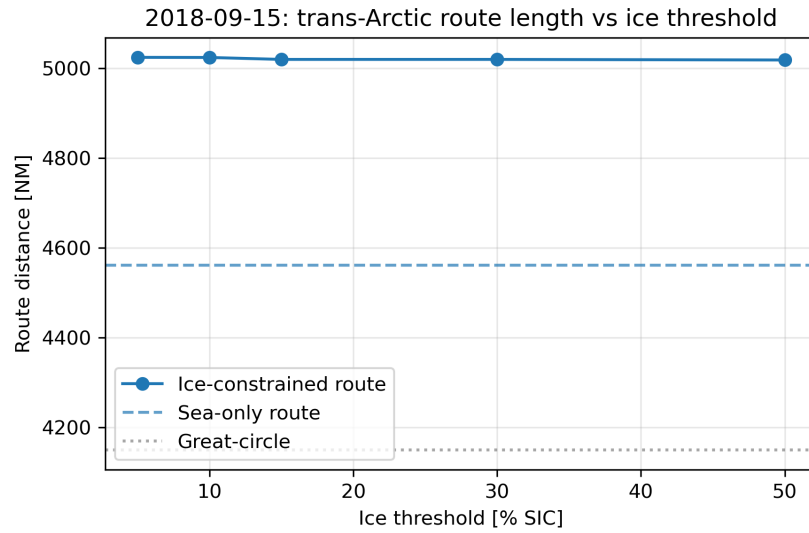


Figure A3: Sensitivity of late-summer (15 September 2018) trans-Arctic route distance to the choice of ice-safety threshold. Solid line: ice-constrained route; dashed line: bathymetry-only sea route; dotted line: great-circle distance.

References

- Aksenov, Y., Popova, E.E., Yool, A., Nurser, A.J.G., Williams, T.D., Bertino, L., Bergh, J., 2017. On the future navigability of arctic sea routes: High-resolution projections of the arctic ocean and sea ice. *Marine Policy* 75, 300–317. doi:10.1016/j.marpol.2015.12.027.
- Chen, X., Shu, Y., Feng, H., Lin, Q., 2021. Climate policy and the future of arctic shipping: Economic and environmental trade-offs between the northern sea route and the suez canal under new emission regulations. *Regional Studies in Marine Science* 97, 102911. doi:10.1016/j.rsma.2025.104597.
- Copernicus Marine Environment Monitoring Service, 2023. Arctic ocean sea ice reanalysis. Copernicus Marine Service Marine Data Store. URL: <https://doi.org/10.48670/mds-00336>, doi:10.48670/mds-00336. accessed via doi:10.48670/mds-00336.
- GEBCO Bathymetric Compilation Group, 2024. The gebco_2024 grid – a continuous terrain model of the global oceans and land. URL: <https://www.gebco.net/data-products/gridded-bathymetry-data/gebco2024-grid>, doi:10.5285/1c44ce99-0a0d-5f4f-e063-7086abc0ea0f. accessed 2025-11-16.
- Kuuliala, L., Kujala, P., Suominen, M., Montewka, J., 2017. Estimating operability of ships in ridged ice fields. *Cold Regions Science and Technology* 135, 51–61. doi:10.1016/j.coldregions.2016.12.003.
- Liu, Q., Wang, Y., Zhang, R., Yan, H., Xu, J., Guo, Y., 2023. Arctic weather routing: A review of ship performance models and ice routing algorithms. *Frontiers in Marine Science* 10, 1190164. doi:10.3389/fmars.2023.1190164.
- Lu, L., Kujala, P., Goerlandt, F., 2021. A method for assessing ship operability in dynamic ice for independent navigation and escort operations. *Ocean Engineering* 225, 108830. doi:10.1016/j.oceaneng.2021.108830.
- Melia, N., Haines, K., Hawkins, E., 2016. Sea ice decline and 21st century trans-arctic shipping routes. *Geophysical Research Letters* 6, 541–546. doi:10.1002/2016GL069315.
- Notz, D., Stroeve, J., 2016. Observed arctic sea-ice loss directly follows anthropogenic CO₂ emissions. *Science* 354, 747–750. doi:10.1126/science.aag2345.

- Pruyn, J.F.J., van Hassel, E., 2022. The impact of adding the northern sea route to the belt and road initiative for europe: A chain cost approach. *Transportation Research Interdisciplinary Perspectives* 15, 100659. doi:10.1016/j.trip.2022.100659.
- Stephenson, S.R., Smith, L.C., Brigham, L.W., Agnew, T., 2013. Projected 21st-century changes to arctic marine access. *Climatic Change* 118, 885–899. doi:10.1007/s10584-012-0685-0.
- Stroeve, J., Kattsov, V., Barrett, A., Serreze, M., Pavlova, T., Holland, M., Meier, W., 2012. Trends in arctic sea ice extent from cmip5, cmip3 and observations. *Geophysical Research Letters* 39, L16502. doi:10.1029/2012GL052676.
- World Meteorological Organization, 2014. WMO Sea-Ice Nomenclature. Technical Report WMO-No. 259. World Meteorological Organization. Geneva, Switzerland. URL: https://globalcryospherewatch.org/wordpress/wp-content/themes/global-cryosphere-watch/files/resources/WMO_ice_nomenclature_vol2.pdf. accessed 7 December 2025.
- Zhang, Y., Sun, X., Zha, Y., Wang, K., Chen, C., 2023. Changing arctic northern sea route and transpolar sea route: A prediction of route changes and navigation potential before mid-21st century. *Journal of Marine Science and Engineering* 11, 2340. doi:10.3390/jmse11122340.
- Zhu, S., Fu, X., Ng, A.K.Y., Luo, M., 2018. The environmental costs and economic implications of container shipping on the northern sea route. *Maritime Policy & Management* 45, 456–477. doi:10.1080/03088839.2018.1443228.